European School of Instrumentation in Particle & Astroparticle Physics

European Scientific Institute

Noble liquid detectors

Introduction

The growing success of noble liquids for building particle detectors results from the following facts :

- they are chemically inert ; (long-term operation)
- they are radiation resistant ; (high-radiation environment, LHC , FCC-pp)
- they can be utilized in ionization or/and scintillation modes ; (auto-triggering)
- their signal yield is relatively high ; (good resolution)
- their industrial availability is good (the world production of xenon is 27 t/y) ;
- they can be easily purified ; (long drift distance)
- they can be used to build complex geometry detectors of increasing size ; (granularity)
- low temperature usely helps in reducing the electronic noise ; (good S/B)
- they constitute homogeneous media with homogeneous response.

A few emblematic examples

NA48 liquid krypton calorimeter (built in the 90's)

Homogeneous LKr calorimeter

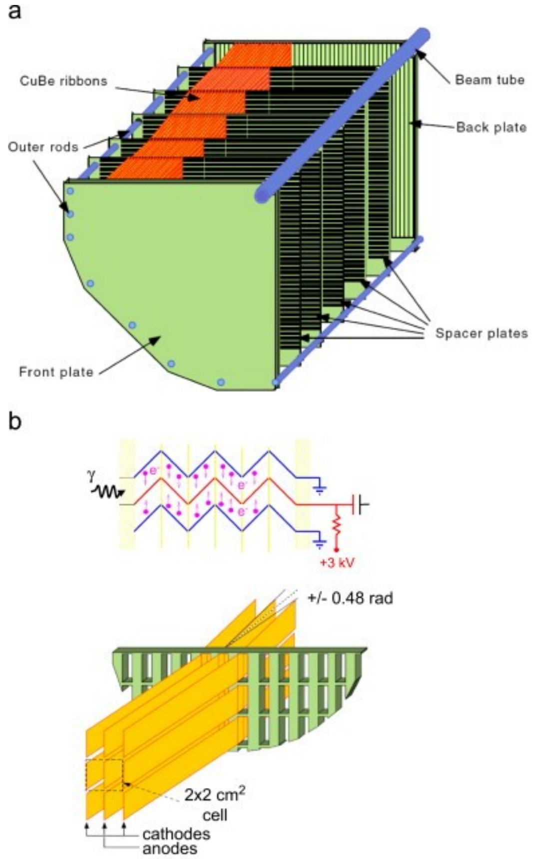

ATLAS liquid argon calorimeter (designed at the beginning of the 90's)

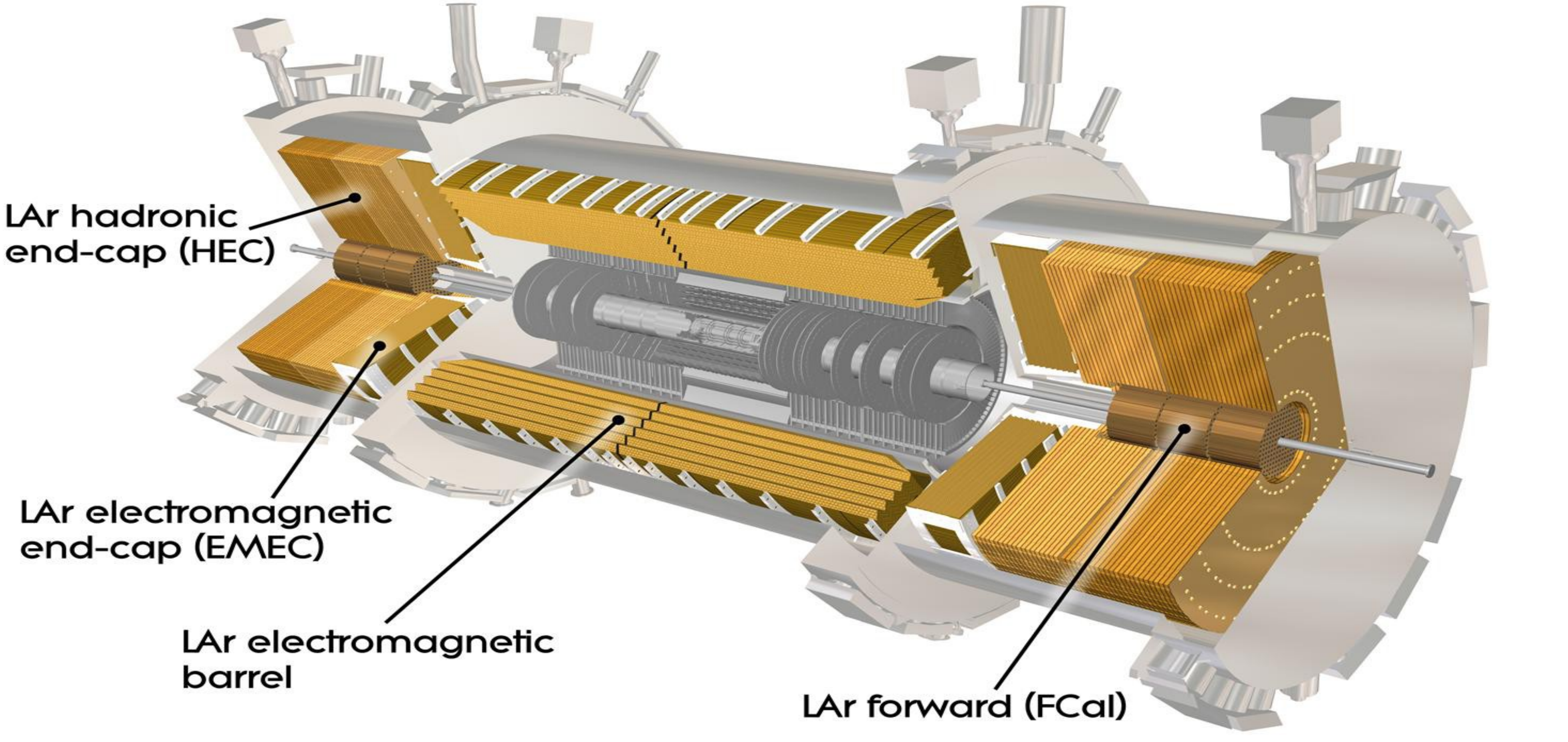

That strongly helped to discover the Higgs boson decaying into two photons

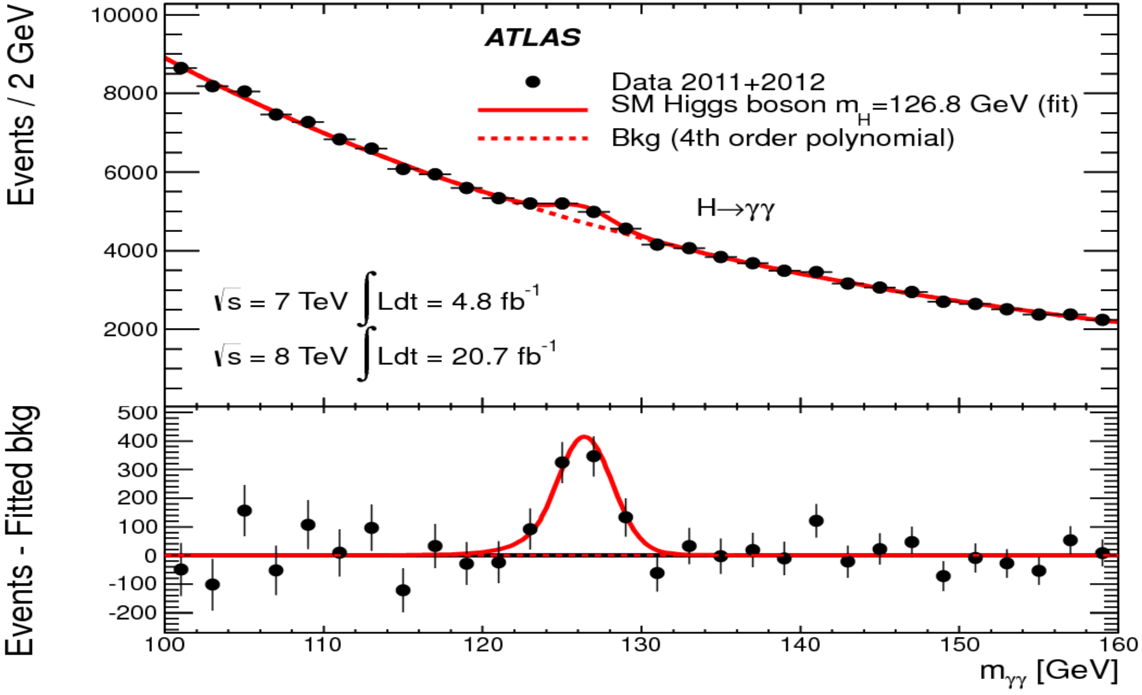

XENON100

100 kg LXe dual-phase TPC

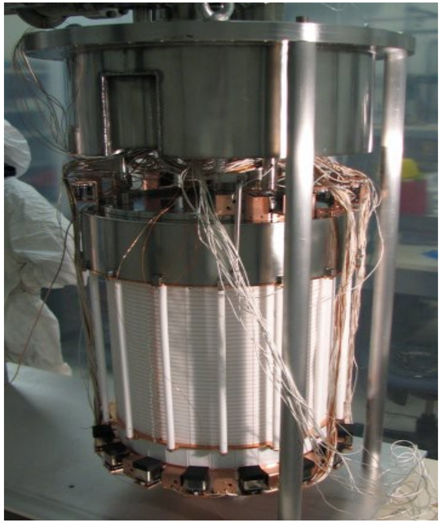

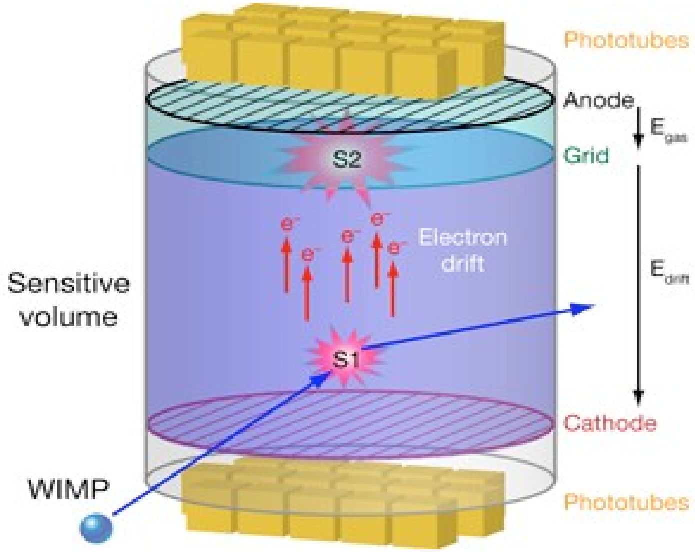

Produced with LUX the most constraining limits to the existence of Wimps

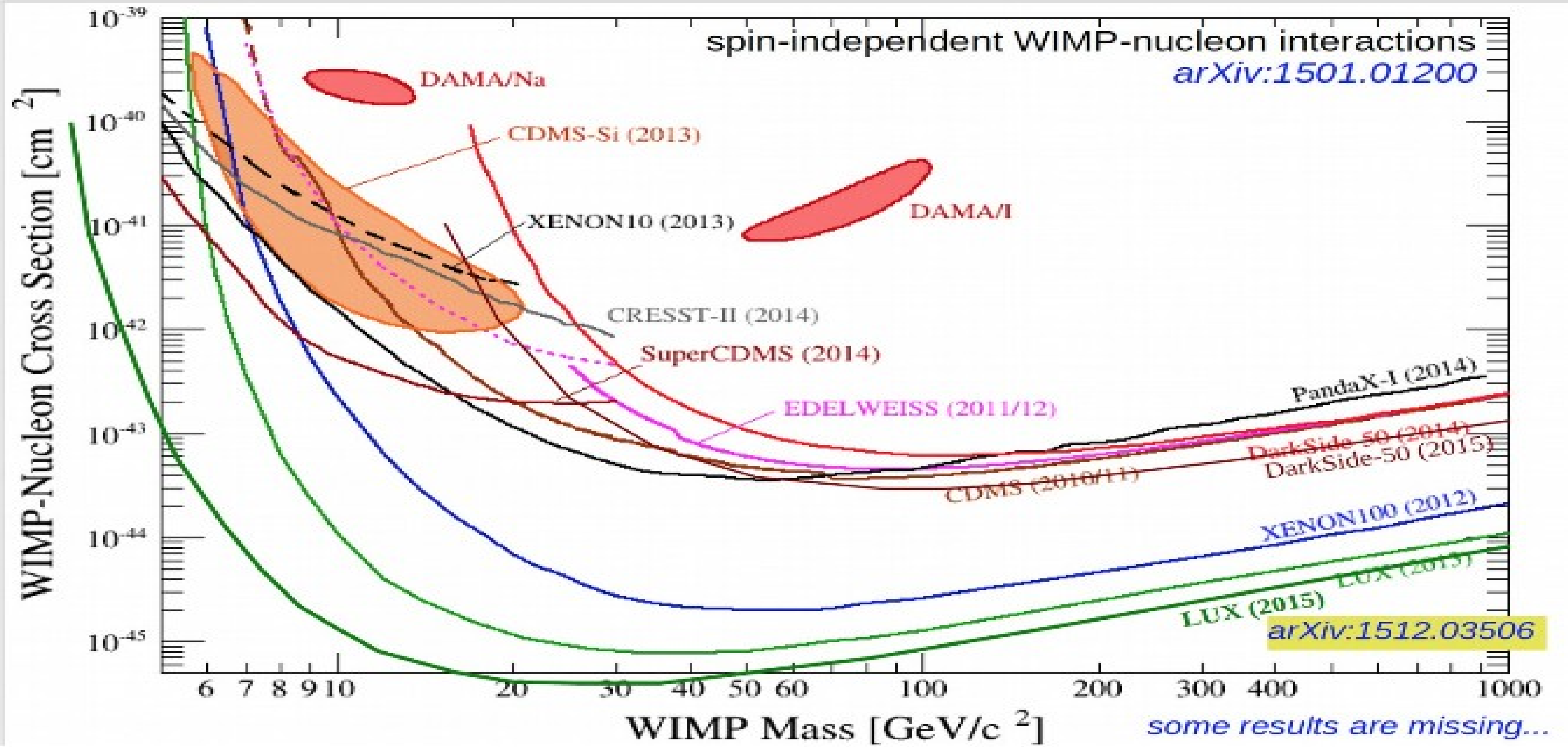

ICARUS

LAr 600 m^3 Time Projection Chamber that was installed in Gran Sasso National laboratory

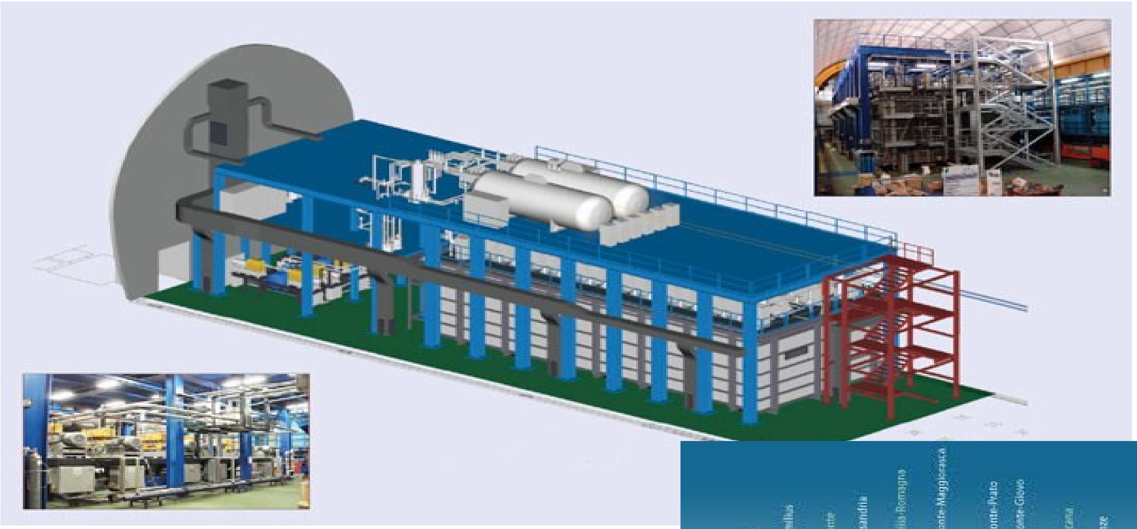

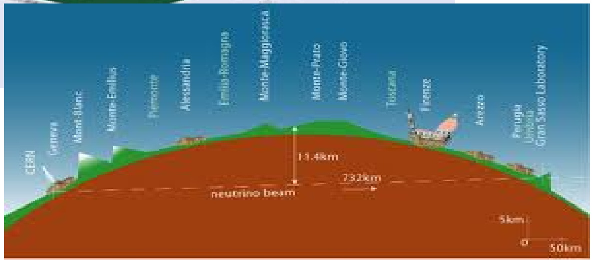

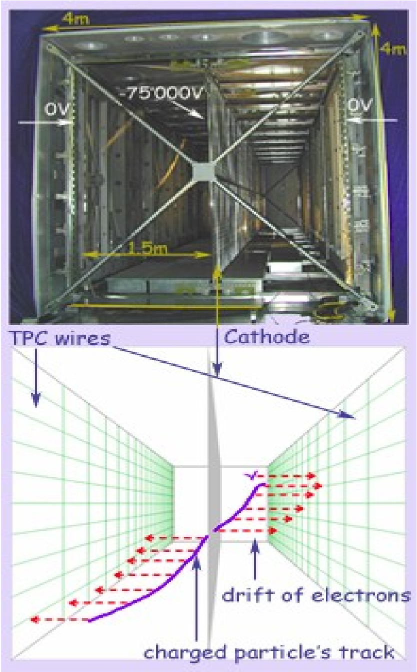

Physical properties

Table of main physical properties

	He	Ne	Ar	Kr	Xe
mol. mass (g mol^{-1})	4.0026	20.183	39.948	83.80	131.3
T_B : boil. temperature at 1 atm. (K)	4.22	27.102	87.26	119.74	169
specific mass at T_b (g cm^{-3})	0.13	1.2	1.399	2.413	3.1
T_S : fusion temperature at 1 atm. (K)		24.55	83.78	115.78	161.36
latent heat at T_B (J Kg^{-1})		87.2	163.2	107.7	96.29
Triple point : temperature (K) pressure (0.1 MPa)		 24.56 0.43	 83.78 0.6876	 115.76 0.734	 161.31 0.8
Critical point : temperature (K) pressure (0.1 MPa)	 5.25 2.26	 44.39 26.86	 150.86 48.9	 209.38 54.27	 289.74 57.64
Thermal conductance at T_B (W m^{-1}K^{-1})	1.6 10^{-5}	0.113	0.125	0.09	0.071

←

Easy to liquify given the fact that T_B > LN_2 temperature (77.3 K)

Vapour pressure curve of argon

Triple point :
83.78 K
0.6876 MPa

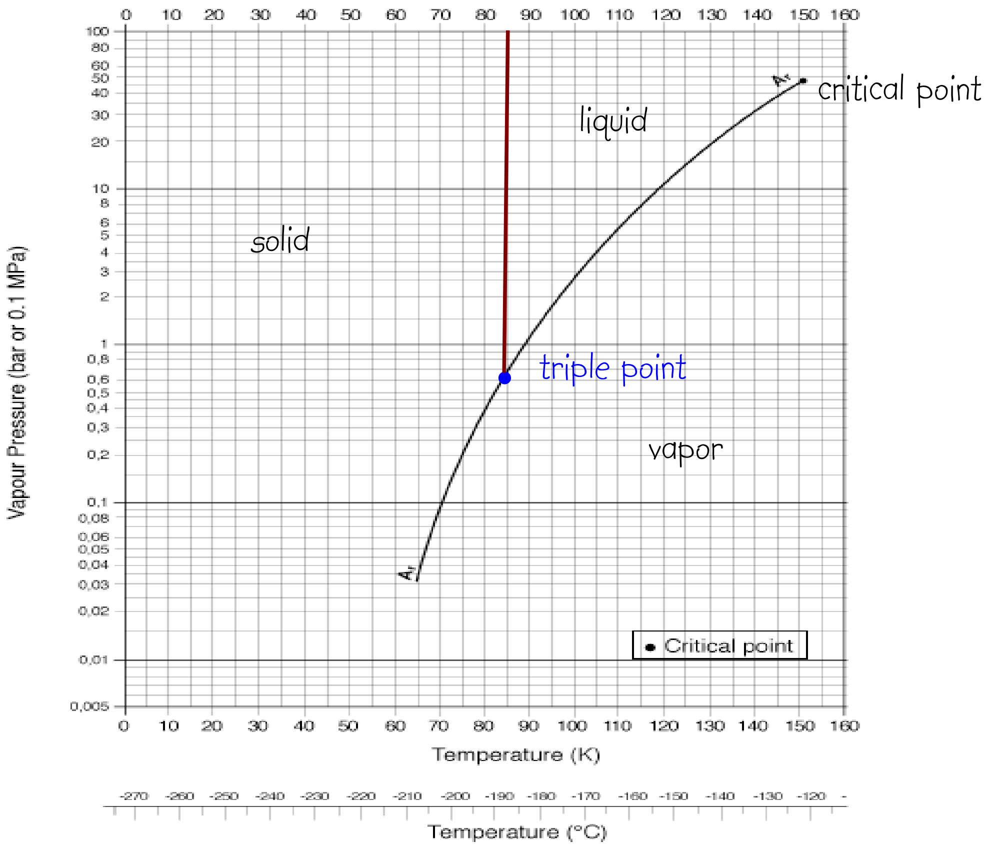

Vapor pressure curve of Krypton

Triple point :
115.76 K
0.734 MPa

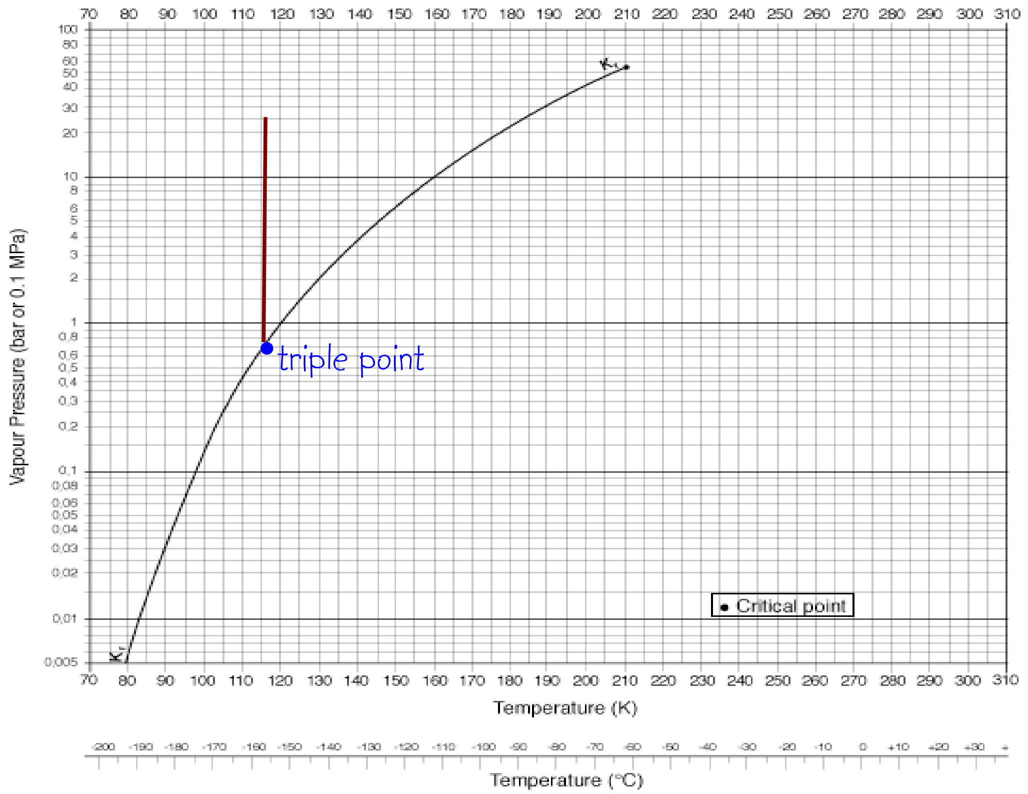

vapor pressure of xenon

Triple point :
161.31 K
0.8 MPa

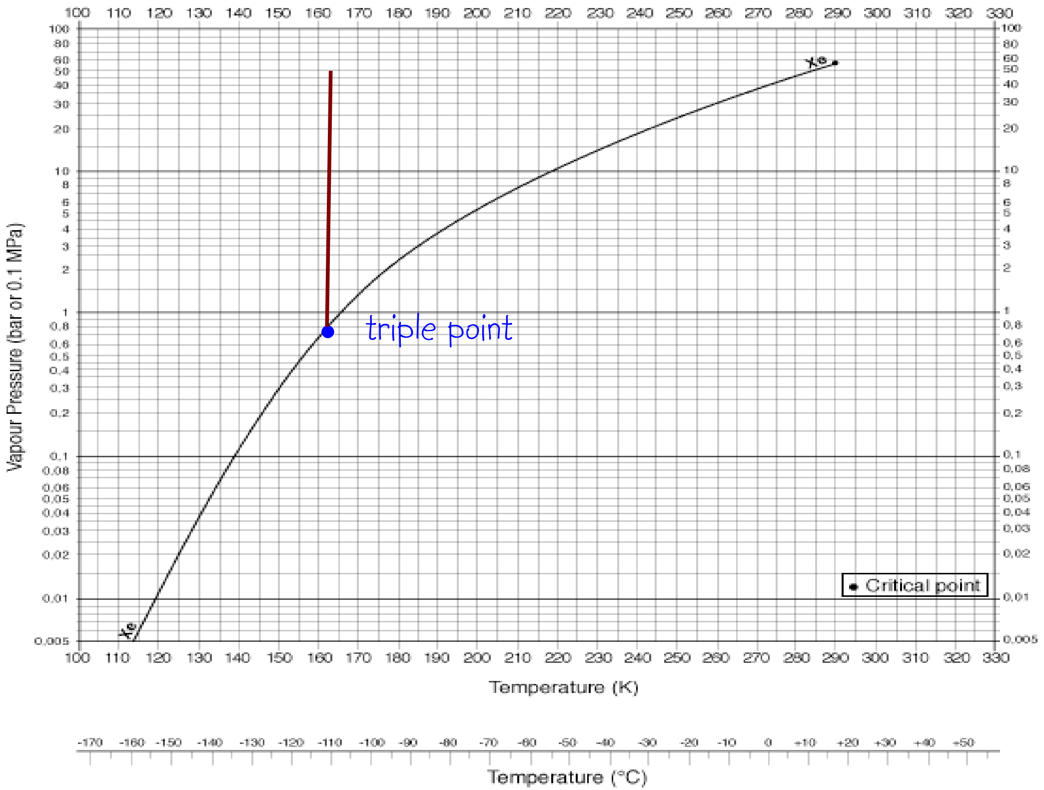

Functional schematic of typical noble liquid detector setup

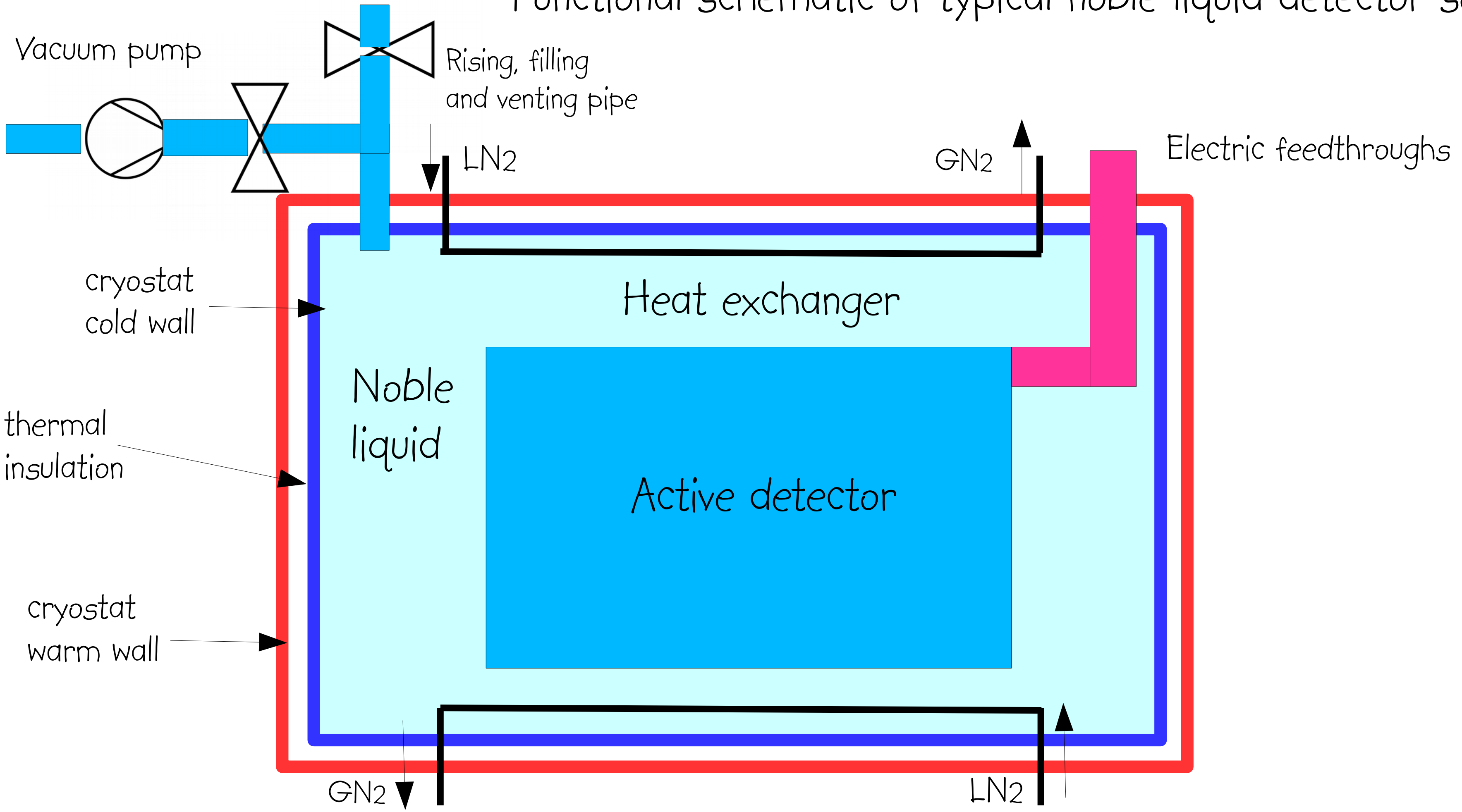

Ionization mode

Noble liquid ionization chamber

$$t_{drif} = d / v_{drift}$$

$$i_0 = \frac{\Delta E}{W_i}\frac{e}{t_{drift}} = \frac{\Delta E}{W_i}\frac{e}{d}V_{drift}$$

$$Q_s = \frac{1}{2} i_0 \, t_{drift} = \frac{Q_i}{2}$$

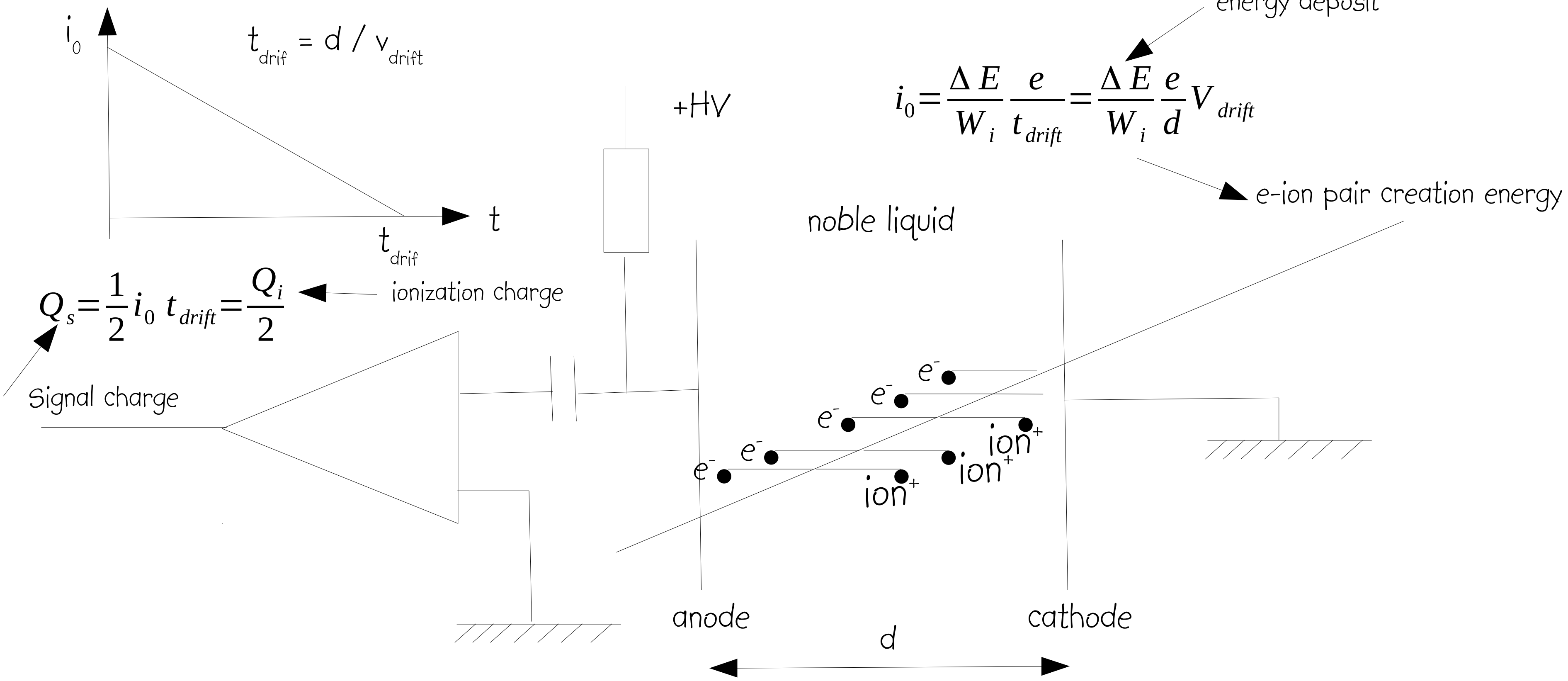

Ionization properties

	LAr	LKr	LXe
dE/dx for a MIP ($\beta\gamma$=3.5) in MeV/cm	2.2	3.5	4
W_i (eV)	23.6 +/- 0.3	18.4 +/- 0.3	15.6 +/- 0.3
V_{drift} at E=10 kV/cm and T_B (mm/μs)	4.75	4.1	2.6
relative dielectric constant	1.6	1.63	1.96

W_i is the energy needed to produce an electron-ion pair in the liquid.

T_B is the boiling temperature.

Electron drift velocity

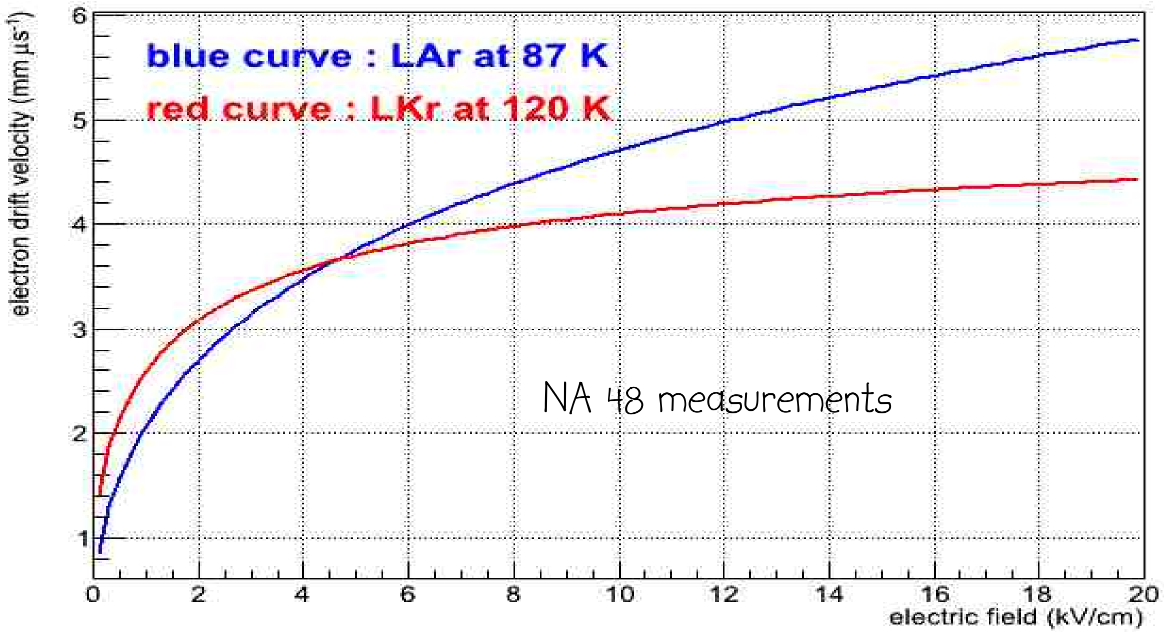

Note that electron drift velocity decreases when T increases : $1/V\ dV/dT \approx -1.5\%\ K^{-1}$

Ion drift velocity is several orders of magnitude smaller. Ion contribution to signal can be neglected.

However ions may contribute to charge build-up if ionization load is too big.

Temperature variation of specific mass

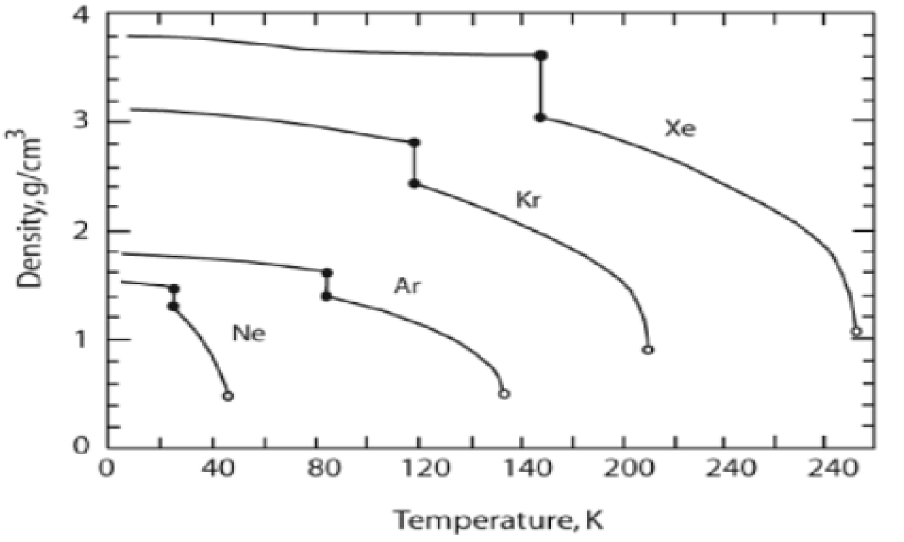

Fig. 2.1 Density of condensed noble gases dependence on temperature (open circles mark critical points, closed circles mark triple points). Redrawn from [18].

ρ diminishes when T increases, hence signal decreases : -0.5% K^{-1}

Recombination of e-ion pairs

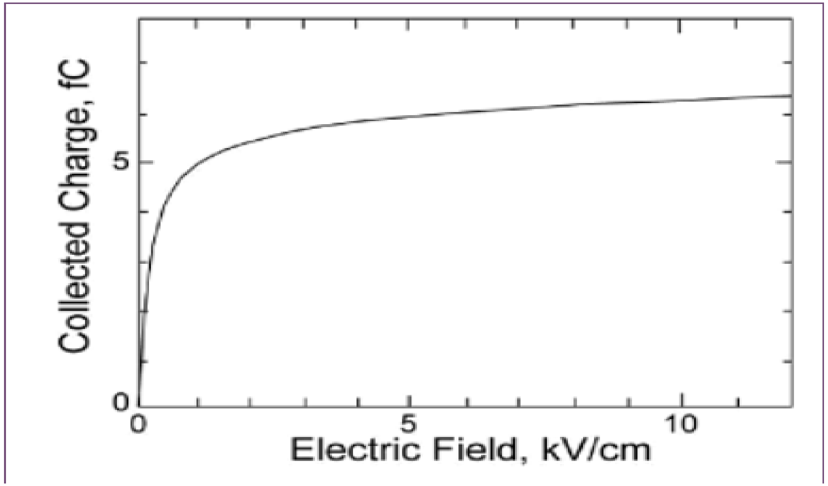

Fig. 2.9 Field dependence of the charge collected from liquid argon ionization chamber irradiated with 976 keV electrons. Redrawn from [60].

If no electric field is applied, all e-ion pairs recombine ! The collected charge progressively rises as a function of electric field and comes to a saturation.

Ionization readout modes

Current mode : readout of initial ionization current.
Differentiation of triangle pulse.
-high-rate capability (LHC)
- but higher electronic noise
-and increased dependence to temperature : -2% K^{-1}
requires temperature control over big volume : $\Delta T < 0.1$ K !

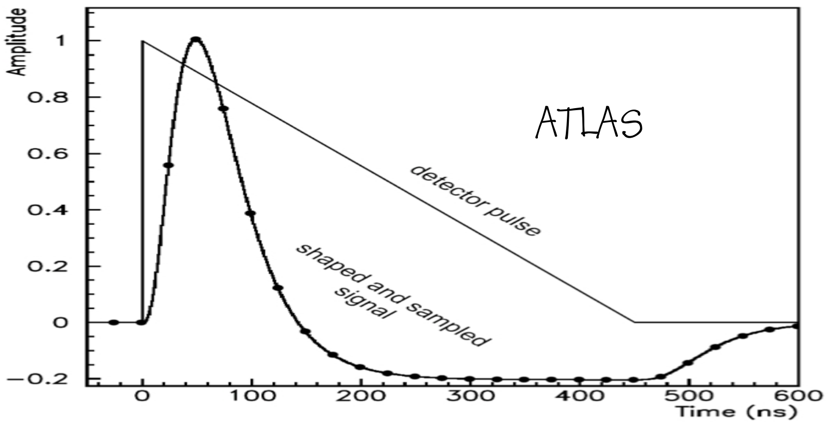

Charge mode : integration of current pulse.
-lower-rate capability (LAr TPC)
-but better noise performance
-and reduced dependence to temperature : -0.5% K^{-1}

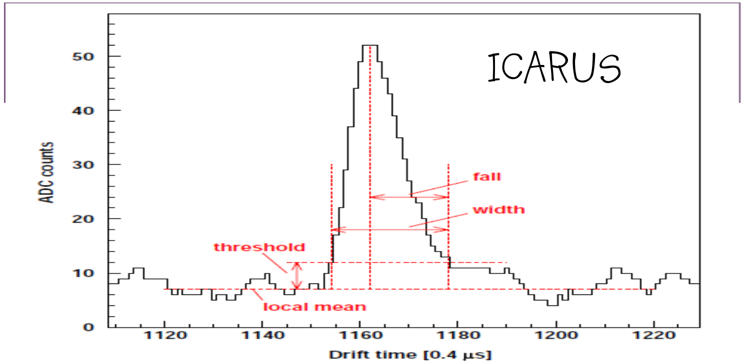

Fig. 68. Example of a hit produced by a minimum ionizing particle on a Collection wire. Marked are the parameters used in the hit search. The output signal has been passed through the low frequency filter.

ICARUS LAr TPC

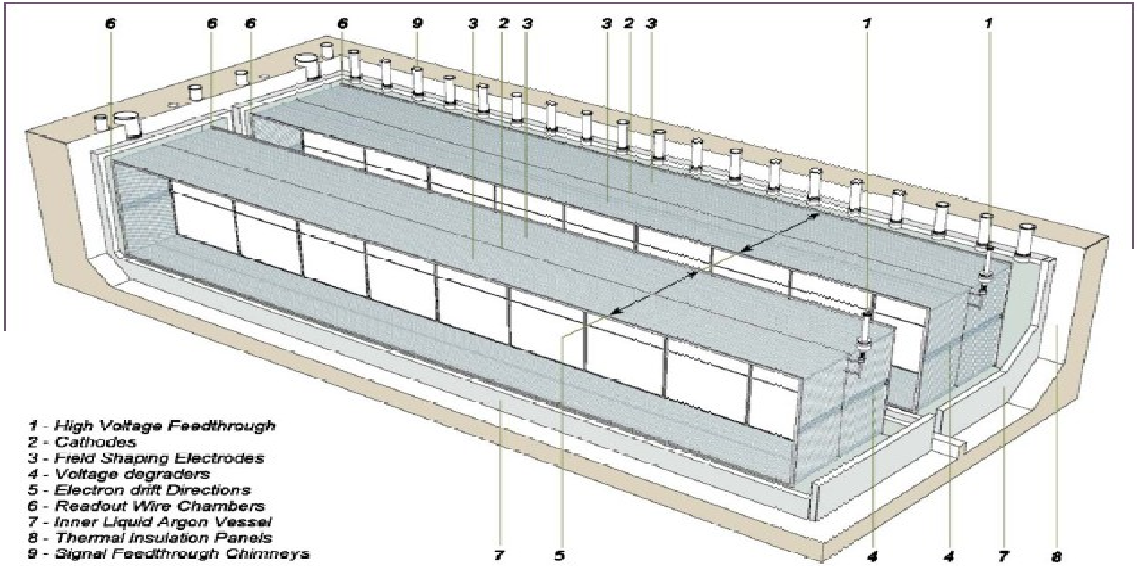

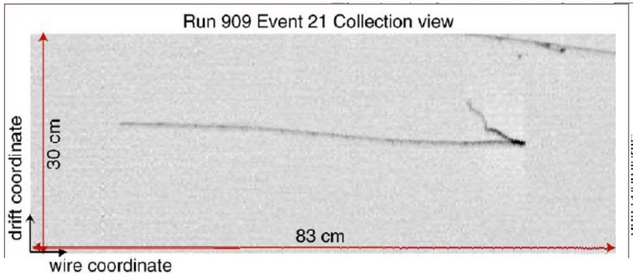

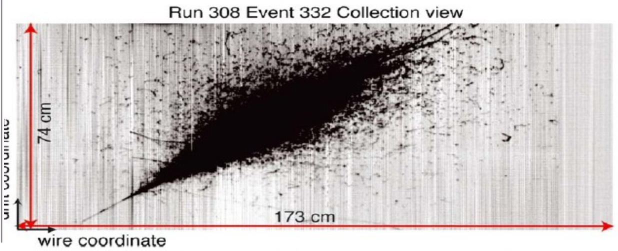

Fig. 66. Run 308, Event 332, Collection view. Electromagnetic shower.

ATLAS LAr electromagnetic calorimeter

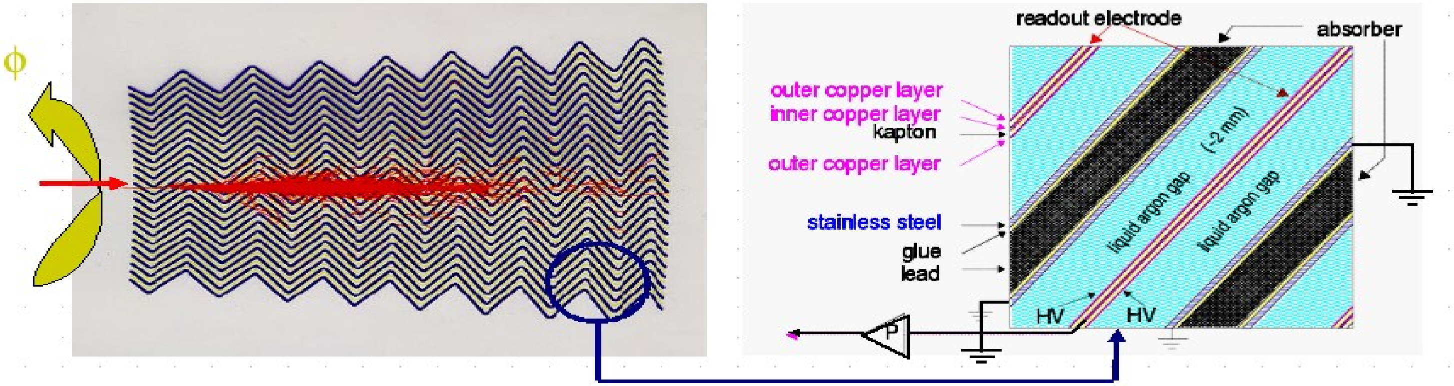

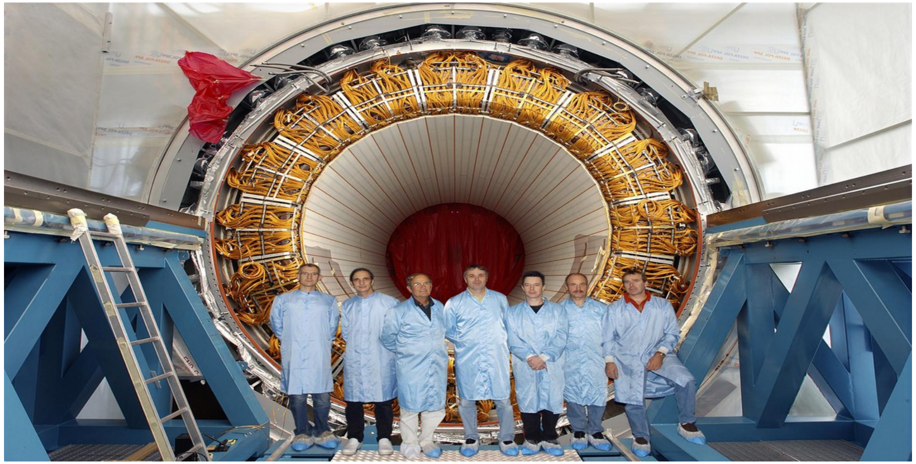

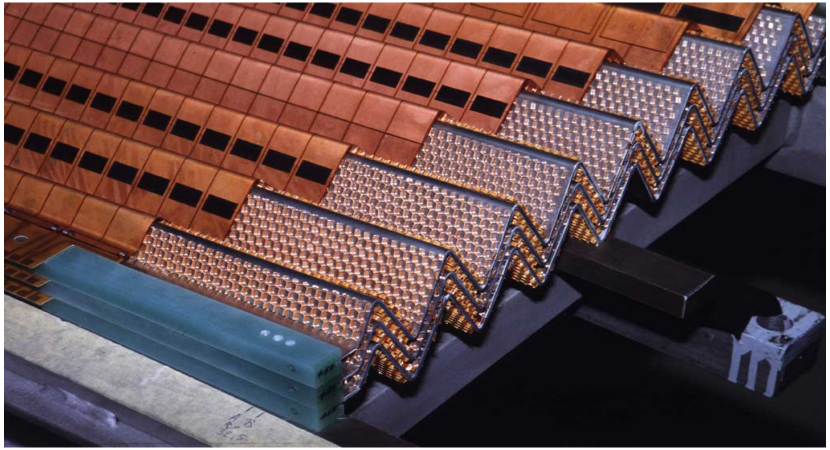

Scintillation mode

Scintillation in LAr and LXe

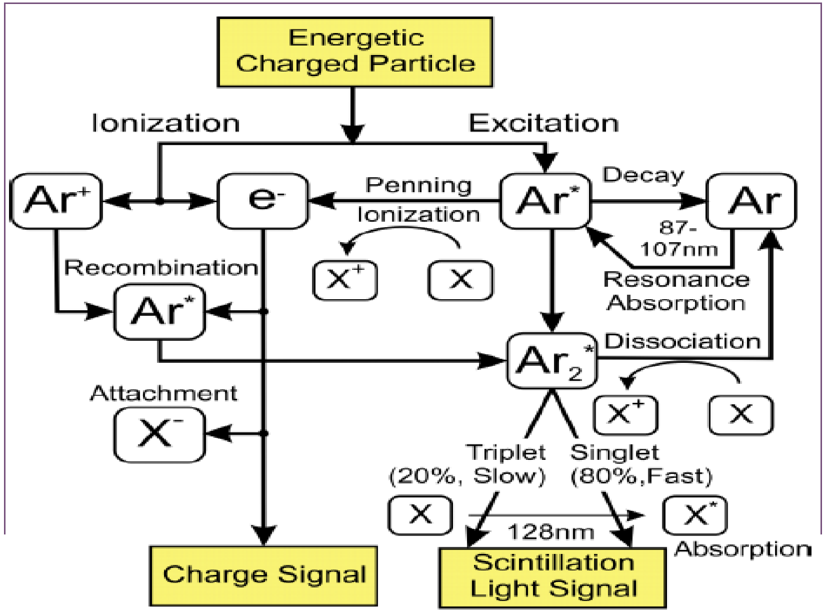

42,000 per MeV

8980 e/mm for MIP (maximum)

51,000 per MeV

10,900 ph/mm for MIP (maximum)

cf. 40,000 for NaI(Tl)

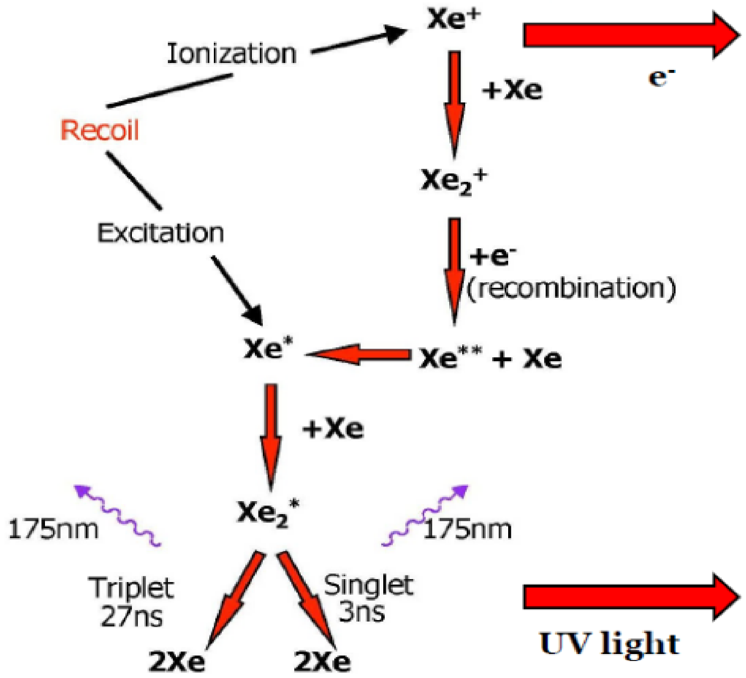

light curves in blue

charge curves in red

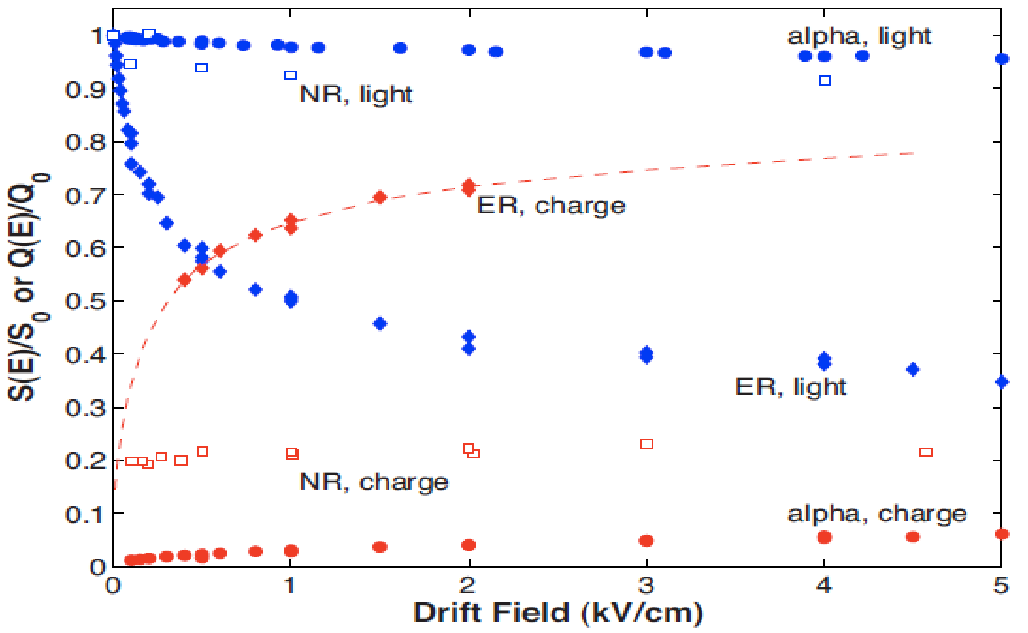

FIG. 6. (Color online) Field dependence of scintillation and ionization yield in LXe for 122 keV electron recoils (ERs), 56.5 keV$_r$ nuclear recoils (NRs) and 5.5 MeV alphas, relative to the yield with no drift field (Aprile *et al.*, 2006).

Light signal diminishes while charge signal increases with electric field

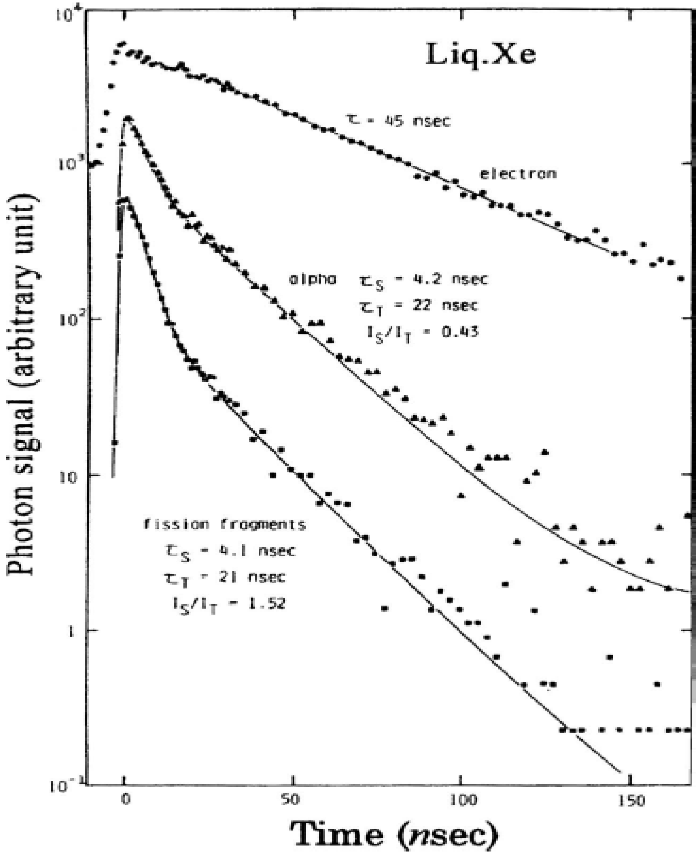

FIG. 19. Decay curves of scintillation from liquid xenon excited by electrons, α particles, and fission fragments, without an applied electric field (Kubota, Hishida, and Ruan, 1978; Hitachi *et al.*, 1983).

scintillation properties

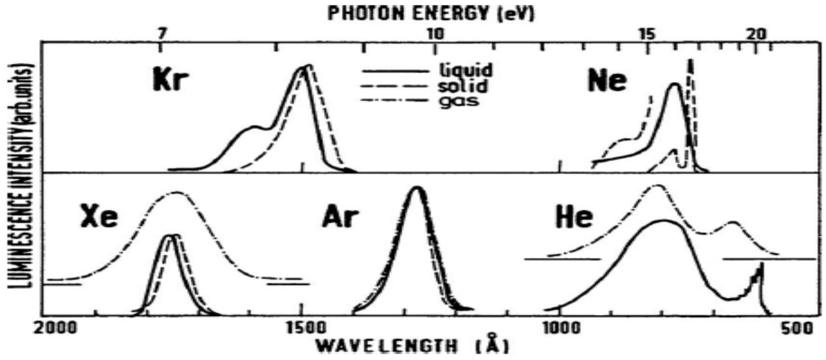

FIG. 18. Emission bands in liquid rare gases, together with solid- and gas-phase spectra (Jortner *et al.*, 1965; Schwenter, Kock, and Jortner, 1985).

	W_{ph} (at zero E field) in eV
LAr	19.5 +/- 1
LKr	15
LXe	13.8 +/- 0.9

W_{ph} is the energy needed to create a UV photon. Note that W_{ph} increases when the electric field is increased.

dual-phase LXe TPC

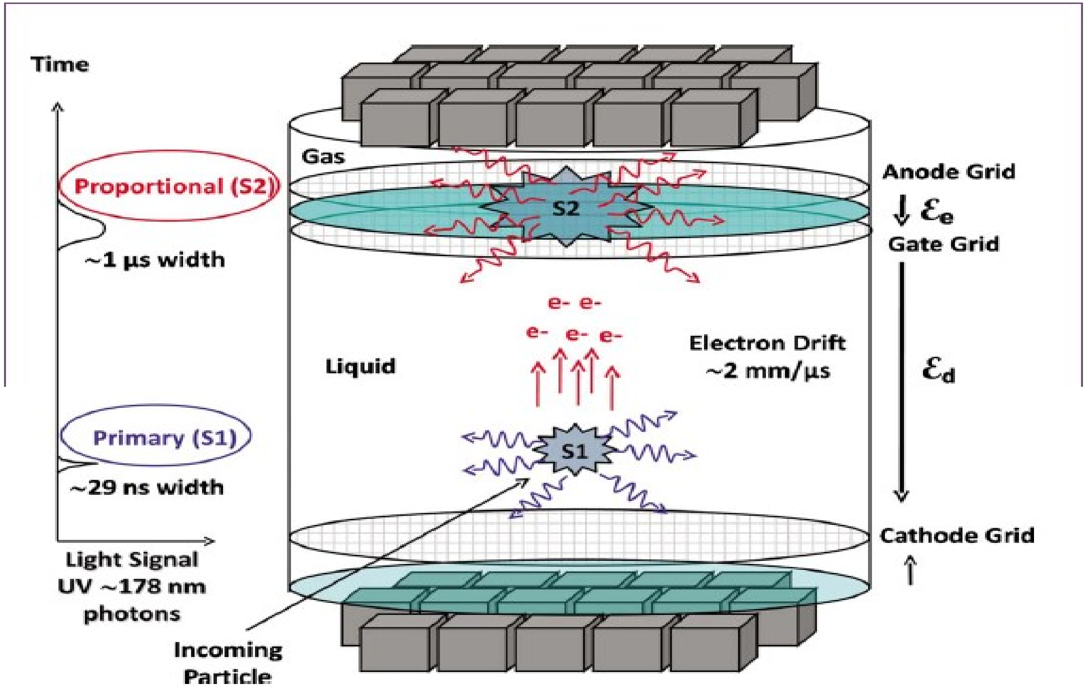

FIG. 44. (Color online) Schematic of a two-phase xenon TPC.

Xenon100

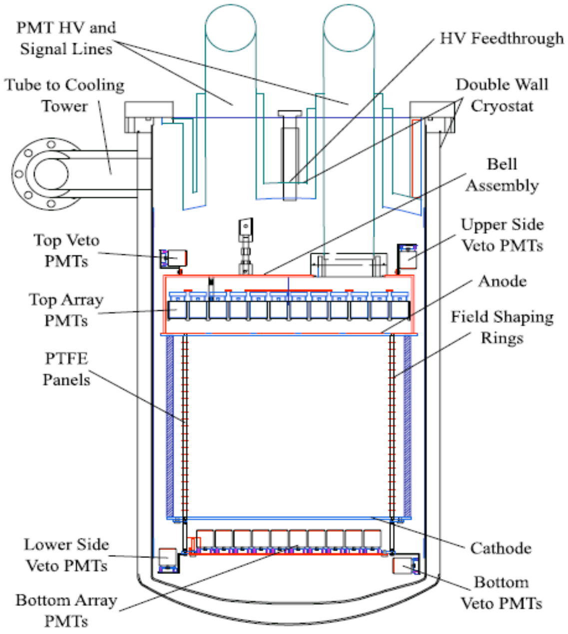

FIG. 56. (Color online) Schematic of the XENON100 detector (Aprile and Baudis, 2008).

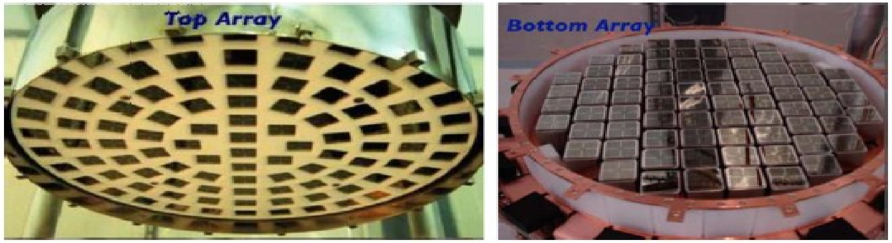

FIG. 57. (Color online) Photos of the top and bottom PMT arrays of the XENON100 detector.

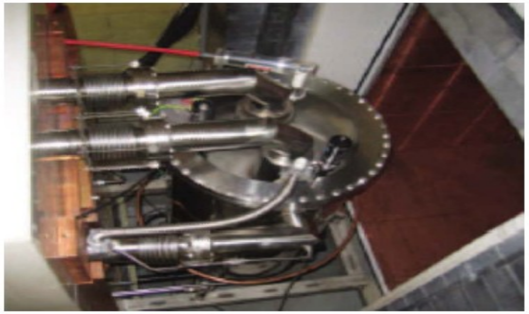

FIG. 58. (Color online) Photo of the XENON100 detector installed in its shield (Aprile, 2008).

XenonIT

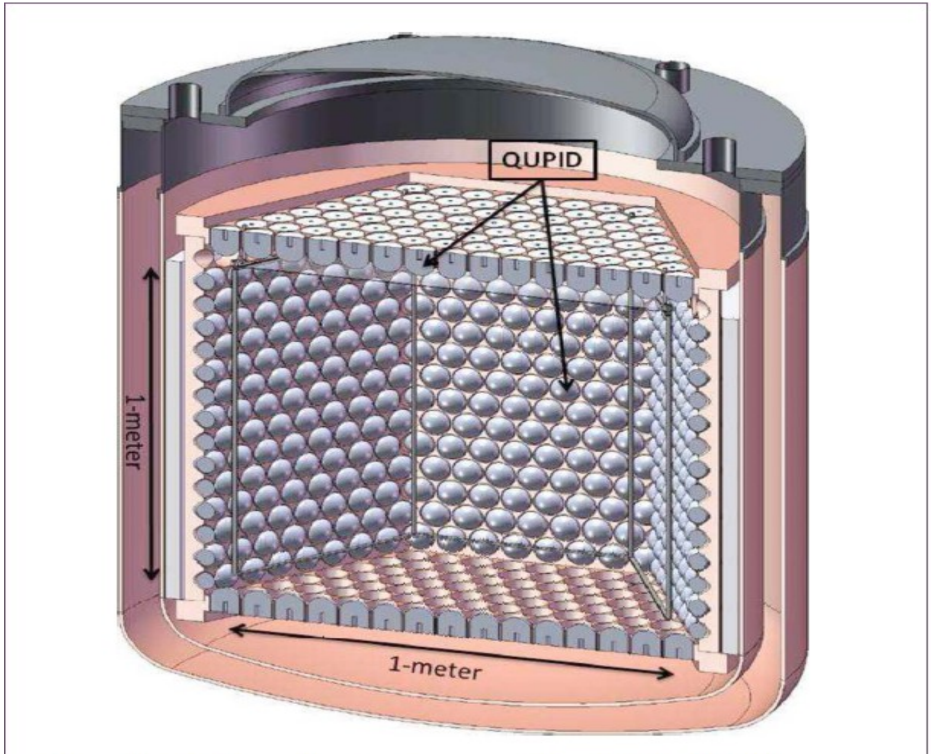

FIG. 59. (Color online) Schematic of the XENON1T detector.

dual-phase noble liquid TPCs

LXe

XENON100

161 kg
≥34 kg

LUX

370 kg
≥118 kg

Panda-X

125 kg
≥25 kg

LAr

ArDM

850 kg
~several 100 kg

DarkSide-50

46 kg
≥37 kg

Current Status and future goals

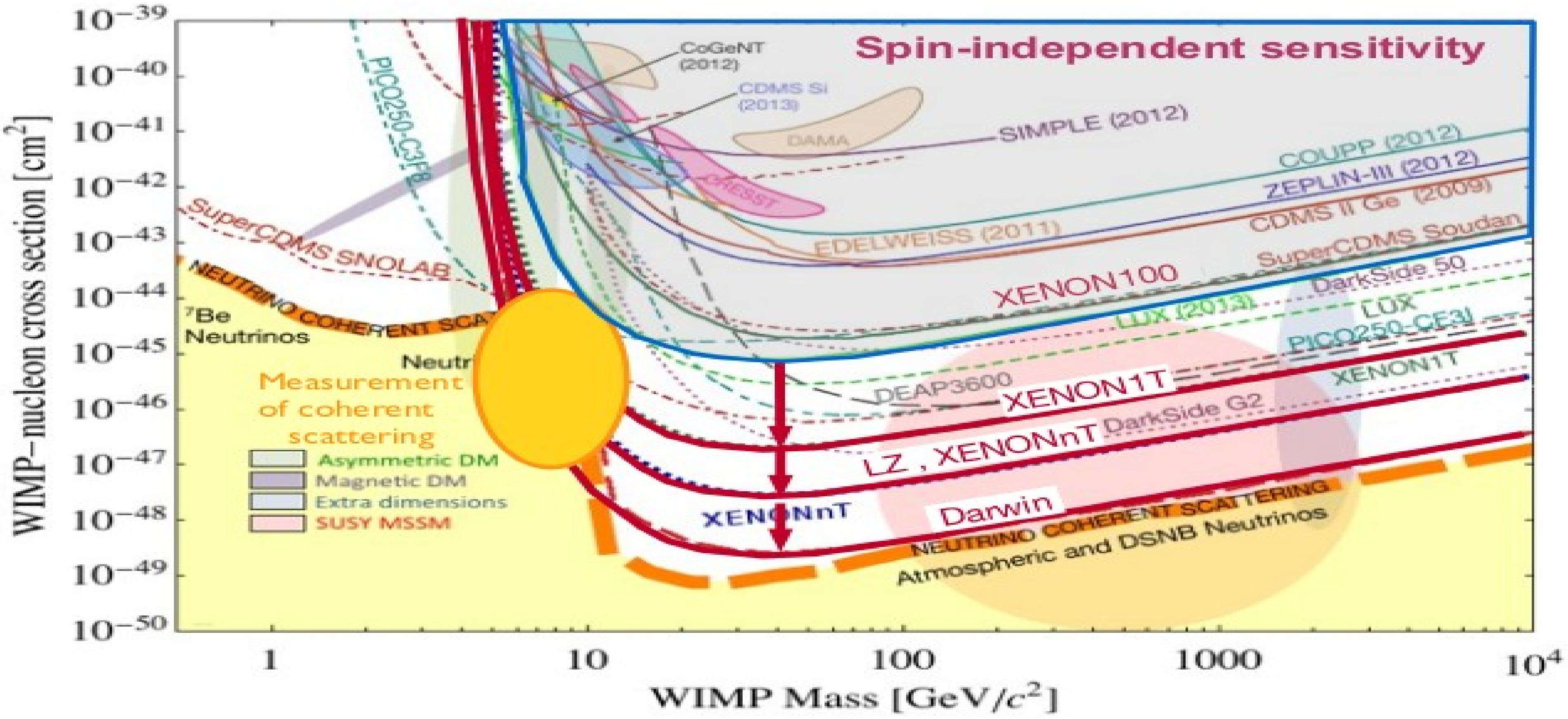

DUNE : Deep Underground Neutrino Experiment

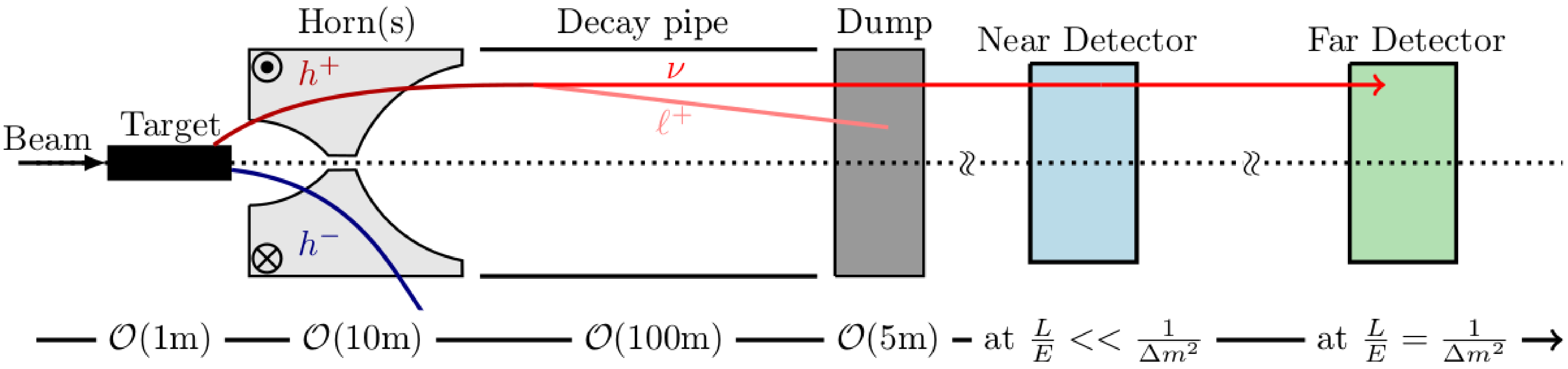

ν_μ and $\bar{\nu}_\mu$ *beams*

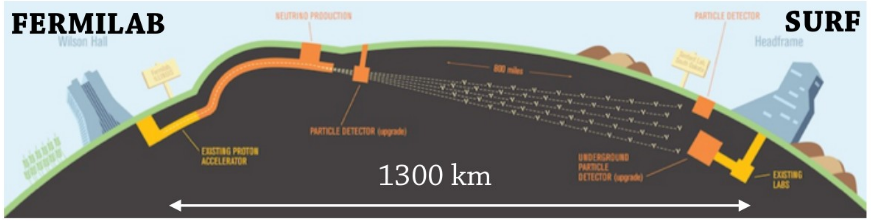

search for CP violation in neutrino oscillations

DUNE Far detector

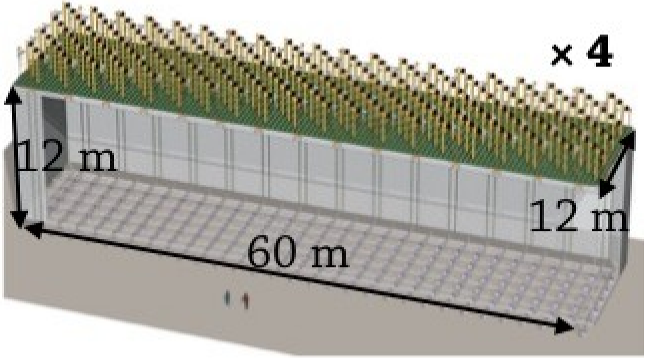

4 modules of 10 kt of LAr each.

First neutrinos in 2026

Single Phase

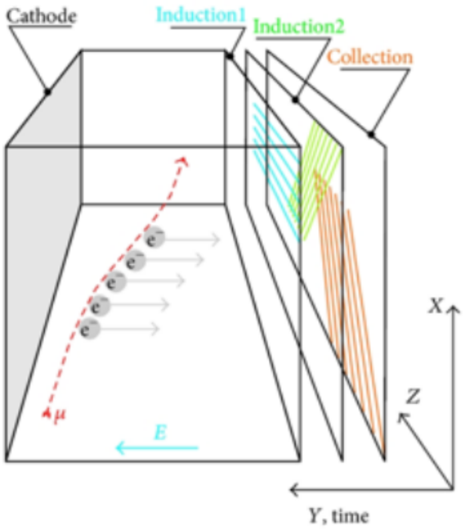

Dual Phase

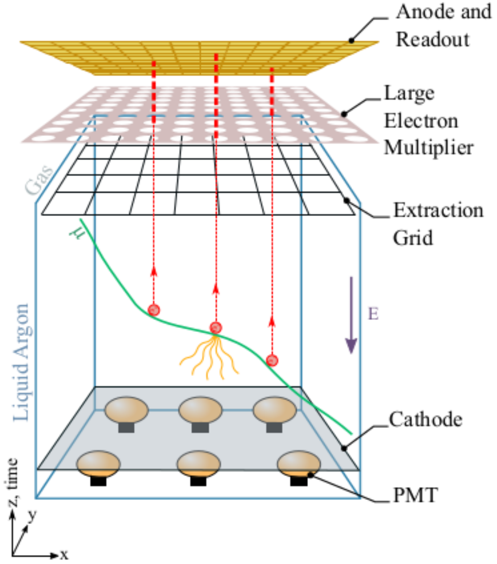

To learn more :

- Noble gas detectors, E. Aprile, A.E. Bolotnikov, A.I, Bolozdynya, T. Doke

- Particle detectors, Claus Grupen, Cambridge monographs on particle physics

- Liquid xenon detectors for particle physics and astrophysics, E. Aprile and T. Doke, Rev. Mod. Phys., Vol 82, No 3, , 2010, 2053

- S. Amerio et al, Design, construction and tests of the ICARUS T600 detector, Nucl. Instrum. and Meth. in physics, A 527 (2004) 329